<div align="center">

QUANTUM
INFORMATICS

Implementation of a Quantum Memory Protocol Based on the Revival of Silenced Echo in Orthogonal Geometry at the Telecommunication Wavelength

</div>

<div align="center">

M. M. Minnegaliev[a],*, K. I. Gerasimov[a], and S. A. Moiseev[a]

[a] Kazan Quantum Center, Kazan National Research Technical University named after A.N. Tupolev, Kazan, 420111 Russia
*e-mail: mansur@kazanqc.org
Received April 11, 2023; revised April 26, 2023; accepted April 29, 2023

</div>

An optical quantum memory protocol has been implemented on the basis of the revival of silenced echo at the telecommunication wavelength for signal light fields with a small number of photons. To this end, a long-lived (>1 s) absorption line has been initialized and the orthogonal geometry of the propagation of the signal and rephasing fields has been chosen. An efficiency of revival of $(17 \pm 1)\%$ has been reached for the orthogonal polarization components of a signal pulse at a storage time of 60 μs. The input pulse contains ~38 photons on average, the revived echo signal includes ~6 photons, and the signal-to-noise ratio is 1.3.

Optical quantum memory (OQM) is designed to store quantum states of light with the subsequent extraction of these states by demand at an arbitrary time. The development of effective multi-qubit OQM at the telecommunication wavelength ($\lambda \sim 1.5$ μm) is one of the key tasks in optical quantum technologies [1], primarily because it is of a great importance for the development of a quantum repeater necessary for long-distance optical quantum communications [2], and it is also considered as an important unit for the development of a quantum Internet network and a universal quantum computer [3]. Various protocols have been proposed during the last two decades to efficiently write and read photon qubits from an OQM cell [4, 5]. An OQM scheme based on an efficient retrieved photon echo in an optically dense medium [6] has been actively applied to the development of some protocols for its implementation in the crystals doped with rare-earth ions [7]. One of such protocols is based on the revival of silenced echo (ROSE protocol) [8] and is developed in this work.

The ROSE protocol is close to the classical two-pulse photon echo scheme, where the signal and rephasing pulses are supplemented with the second rephasing pulse, which recovers the primary echo signal, which is emitted in the already uninverted system [9]. The ROSE signal reaches a maximum when rephasing light pulses have a pulse area of π, which coincides with the Carr–Purcell sequence known in NMR studies [10]. At the same time, unlike echo signals in the Carr–Purcell sequence, primary photon echo is completely suppressed in the ROSE protocol, and almost the entire energy stored in atoms is emitted

in the ROSE signal at the exact implementation of the protocol. The development of the ROSE protocol under various experimental conditions is promising because of a relative simplicity of its implementation and a long quantum coherence time in it. Primary echo is suppressed by different methods, e.g., by controlling phase matching conditions through the choice of the propagation direction of the signal and rephasing laser fields, as shown in [8, 11, 12], or by means of the additional control of the rephasing of atomic coherence [13–15]. The ROSE protocol has been recently implemented in a cavity in the impedance-matching regime with the address record and the read-out of signal pulses [16]. Experimental developments of the ROSE protocol in integrated structures were reported in [17, 18].

The authors of experimental works [8, 11, 12, 16–18] used optical transitions in thulium ($\lambda \sim 793$ nm) and europium ($\lambda \sim 580$ nm) non-Kramers rare-earth ions; their application at the telecommunication wavelength is very complicated. The $^4I_{15/2}-{}^4I_{13/2}$ optical transition in erbium ions is of great interest for applications because its wavelength in the Y_2SiO_5 crystal is $\lambda \sim 1.5$ μm, which is in the transparency range of the standard telecommunication optical fiber. The ROSE protocol was implemented with a highest efficiency of 40% in this crystal with the collinear geometry of propagation of light pulses [19, 20]. In those works, pulses with amplitude and frequency modulation were the most appropriate as rephasing pulses [16, 21]. However, even these pulses did not ensure a sufficiently high degree of inversion of resonance transi-

tions in the real experiment with an ensemble of two-level atoms; as a result, very undesired spontaneous emission occurred during the emission of the ROSE signal. One of the ways to reduce luminescence-induced quantum noise is the modification of the absorption line of the inhomogeneously broadened transition, which leads to the appearance of the residual population of excited atoms only in the spectral range of the signal pulse [16]. To use the ROSE protocol in practice, the modified absorption line should have a sufficiently long lifetime. It is noteworthy that it is not difficult to create long-lived spectral holes for non-Kramers ions (such as Eu^{3+}, Pr^{3+}, ...) with zero electron magnetic moment because their hyperfine sublevels have long lifetimes T_1, e.g., $T_1 = 23$ day for europium ions in the Y_2SiO_5 crystal [22].

Kramers ions (such as Er^{3+}, Nd^{3+}...) can be characterized by the effective electron spin $S = 1/2$. The fast relaxation of the electron spin typical of these ions significantly reduces the lifetime of hyperfine states in them. At the same time, the authors of [23, 24] showed that transitions between electron−nuclear sublevels of the ground state of $^{167}Er^{3+}$ in the Y_2SiO_5 crystal can have long lifetimes and spin coherence times (several to several tens of seconds) under the additional suppression of electron spin relaxation processes. Such a suppression can be ensured by placing the crystal in high magnetic fields ($H > 3$ T) at low temperatures ($T < 1.5$ K), at which the electron spin in the ground state is almost completely "frozen," so that relatively fast spin relaxation weakly affects the relaxation of nuclear spins [23]. Optical transitions of $^{167}Er^{3+}$ ions in the Y_2SiO_5 crystal at a wavelength of $\lambda \sim 1538.3$ nm (site 2) occur between the eight lowest hyperfine sublevels of the ground Kramers doublet and eight hyperfine sublevels of the optically excited doublet. In this case, the absorption spectrum consists of three groups of lines corresponding to optical transitions with a change in the nuclear spin projection by $\Delta m_I = m_I(\text{g}) - m_I(\text{e}) = -1, 0, +1$. The hyperfine structure in the observed absorption spectrum is quite well optically resolved, which allows one to step-by-step transfer the entire ensemble of ions to one long-lived hyperfine state and to create a high nuclear spin polarization by optical pumping [24]. This initial state in the ensemble of $^{167}Er^{3+}$ ions provides rich possibilities of improving the basis parameters of the ROSE protocol, which is the aim of this work.

In this work, we experimentally implement the ROSE protocol in the $^{167}Er^{3+}$:Y_2SiO_5 crystal using the orthogonal geometry of propagation of signal and rephasing pulses with the preparation of the initial absorption spectrum on the $^4I_{15/2}(0)-^4I_{13/2}(0)$ optical transition in erbium ions in order to reduce quantum noise in the studied OQM protocol. Compared to the collinear geometry of propagation of signal and rephasing pulses, orthogonal geometry has the follow-

ing advantages. First, rephasing pulses are less distorted in the process of propagation in an optically dense medium because the signal beam can pass near the edge of the crystal. Second, this geometry ensures a better spatial isolation from scattered photons in a rephasing beam. Third, orthogonal geometry is the most convenient for the subsequent use of the cavity for the signal beam.

The simplified scheme of the quantum transitions in $^{167}Er^{3+}$ ions is presented in Fig. 1a. The sketch of the experimental setup is shown in Figs. 1b and 1c. Figure 2 presents the time sequences of the used laser pulses. The sources of laser radiation were two tunable single-frequency diode lasers tuned to the wavelength $\lambda = 1538.35$ nm of the used optical transition in erbium ions (site 2). The population was redistributed between hyperfine sublevels of the ground state in erbium ions using a diode laser (New Focus TLB-6700, Fig. 1c). The radiation of this laser was modulated in frequency and was passed through an erbium-doped fiber amplifier (Keopsys CEFA-C-PB-LP-SM), where it was amplified to a power of about 80 mW in a continuous mode before entering the cryostat with the $^{167}Er^{3+}$:Y_2SiO_5 crystal. The laser was tuned to optical transitions in erbium with the nuclear spin flip $\Delta m_I = -1$ (indicated by lilac arrows in Fig. 1a and by the horizontal lilac square bracket in Fig. 3). The time of population redistribution between hyperfine sublevels was set to 500 ms (Figs. 2a). To form sequences of light pulses shown in Figs. 2b−2d, we used another master laser (Toptica CTL-1500) whose frequency was stabilized using a servo controller (Vescent Photonics D2-125) by an optical reference with a high finesse ($F > 1000$) and a high thermal stability (<5 MHz/K) of the resonance frequency. The sequences of signal and probe pulses (shown in Figs. 2c and 2d, respectively) were formed from the radiation of the master laser using an acousto-optic modulator (AOM in Fig. 1c). A fraction of laser radiation was additionally amplified by the erbium-doped fiber amplifier (up to 180 mW in front of the cryostat). Amplified radiation passed through the fiber acousto-optic modulator (FAOM in Fig. 1d), which formed the sequences of pulses used to modify the absorption line and to form rephasing pulses (see Fig. 2b). The sequences of pulses presented in Fig. 2 were repeated with a frequency of 0.5 Hz.

The $3 \times 3 \times 5$-mm rectangular parallelepiped $^{167}Er^{3+}$:Y_2SiO_5 ($c = 0.005\%$) crystal with edges parallel to the $D_1 \times D_2 \times b$ axes, respectively (shown in the inset of Fig. 1b), was cooled to a temperature of 1.3 K in a closed-cycle cryostat with a superconducting magnet. A magnetic field of $H = 3.39$ T was directed along the D_1 axis of the crystal. The signal light pulse $\mathbf{E}_s$ propagated parallel to the D_1 axis of the crystal ($\mathbf{E}_s \parallel D_1 \parallel \mathbf{H}$, turquoise horizontal line in Fig. 1b) and
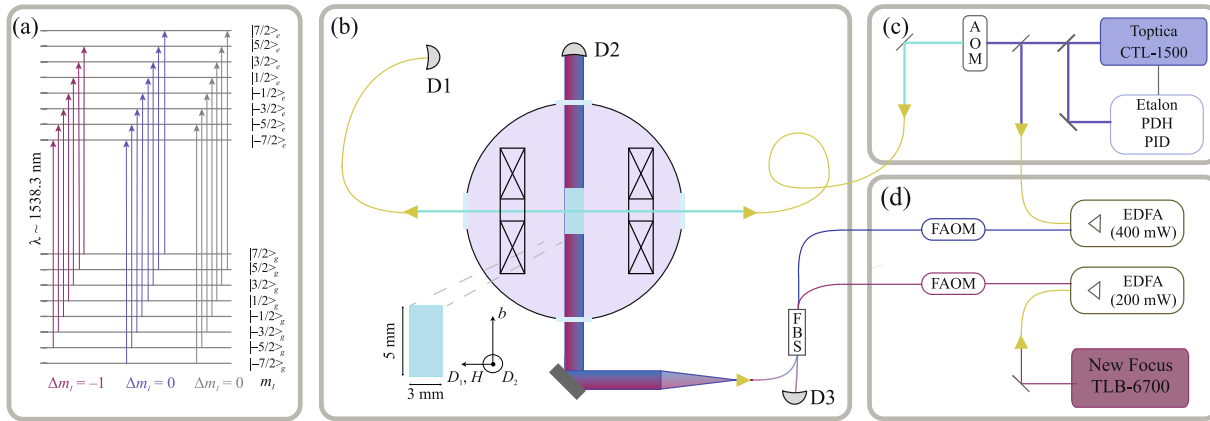
Fig. 1. (Color online) Simplified sketch of the experimental setup. (a) Scheme of quantum transitions between the energy levels of $^{167}Er^{3+}$. (b) $^{167}Er^{3+}$:Y_2SiO_5 crystal in a cryostat at a temperature of 1.3 K in an external magnetic field of $H = 3.39$ T: (yellow triangles) input/output of radiation to/from the optic fiber, (D1, D2, D3) detectors, (FBS) 50 : 50 fiber beam splitter. (c) Unit for the preparation of the signal and probe fields; a fraction of radiation is guided to unit (d) to modify the absorption line and to generate rephasing pulses; (AOM) acousto-optic modulator of light. (d) Unit for the preparation of rephasing pulses using a Toptica CTL-1500 laser and laser radiation for the redistribution of erbium ions in the ground state using a New Focus TBL-6700: (EDFA) erbium fiber optic amplifier and (FAOM) fiber acousto-optic modulator of light.
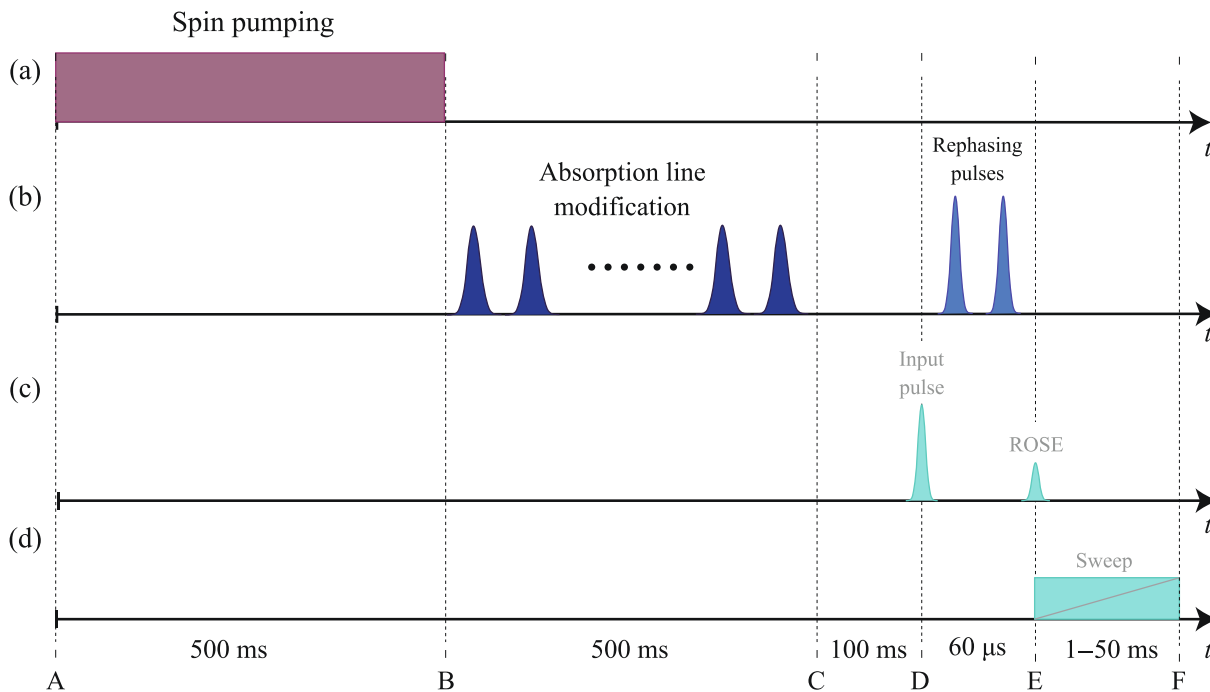

Fig. 2. (Color online) Time sequence of light pulses. (a) Long radiation pulse (spin pumping) in the interval A−B ensuring the redistribution of the population between hyperfine sublevels of the ground state of erbium ions. (b) Sequence of pulses for the initialization of the initial absorption spectrum in the interval B−C and for the generation of rephasing pulses in the interval D−E. (c) Time of the start of the signal pulse D and the time of the emission of the ROSE signal E. (d) Probe radiation in the interval E−F probing the absorption spectrum in the working spectral range.

was polarized either along the D_2 ($\mathbf{E}_s \parallel D_2$) or b ($\mathbf{E}_s \parallel b$) axes of the crystal. Light pulses whose sequences are shown in Figs. 2a and 2b propagated along the 5-mm-long edge of the crystal parallel to the b axis. Light pulses were polarized along the D_1 axis of the crystal.

To measure the input signal pulse and the emitted ROSE signal, we used a photodetector (D1 in Fig. 1a) based on an avalanche photodiode (Thorlabs APD110C/M), a signal from which was fed to an oscilloscope (Tektronix DPO 7104C). In experiments with

signal pulses with a small number of photons, a superconducting single-photon detector (Scontel SSPD) was used instead of the avalanche photodiode. In these experiments, a fiber filter (SKEO SK-CF55M) was also added to the detecting channel in order to cut radiation with wavelengths corresponding to luminescence from the $^4I_{13/2}(0)$ excited optical level to the $^4I_{15/2}(n = 1, 2)$ excited levels of the ground multiplet. The wavelengths of luminescence to the other $^4I_{15/2}(n > 2)$ erbium levels were beyond the working spectral range of the detector. Thus, radiation with frequencies corresponding to the resonance luminescence line that are in the OQM frequency range reached the photodetector D1.

Figure 3 shows the experimental data on the kinetics of population redistribution between hyperfine sublevels of the ground state of $^{167}Er^{3+}$ ions predominantly to the $m_I = -7/2$ state in terms of the B–E time delay between the redistributing (Fig. 2a) and probe (Fig. 2d) pulses, which is indicated in seconds in the legend in the upper right part of Fig. 3. The inset of Fig. 3 shows the decrease in the absorption intensity (state population) of the most intense line near 0 GHz with increasing time delay of the probe radiation. The presented experimental data on the kinetics of the absorption decrease are described well by the sum of two exponentials $\alpha L(\tau_{BE}) = \alpha L_{np} + A_1 e^{\frac{-\tau_{BE}}{T_{middle}}} + A_2 e^{-\frac{\tau_{BE}}{T_{slow}}}$ with the parameters $T_{middle} = (2.5 \pm 0.3)$ s, $T_{slow} = (10.3 \pm 2)$ s, $A_1 = 1.42$, $A_2 = 1.25$, and $\alpha L_{np} = 1.67$. This approximation is represented by the red solid line in the inset of Fig. 3. It is worth noting that the measured time T_{slow} coincides within a high accuracy with the value obtained in [25] in the $^{167}Er^{3+}:Y_2SiO_5$ crystal for the first impurity center at $T = 1.6$ K in the absence of the external magnetic field.

Further, we prepared the initial absorption spectrum on the optical transition with the selection rule $\Delta m_I = 0$ between hyperfine sublevels of the ground and $m_I = -7/2$ excited states using the sequence of two burning laser pulses presented in the B–C interval in Fig. 2b. These pulses were amplitude and frequency modulated [16, 21], and their electric fields $\varepsilon_p(t)$ and carrier frequencies $\omega_p(t)$ had the form

$$\varepsilon_p(t) = \varepsilon_0 \text{sech}\left(\beta(t - t_p)\right), \tag{1}$$

$$\omega_p(t) = \omega_{0,p} + \mu\beta \tanh\left(\beta(t - t_p)\right), \tag{2}$$

where $p = 1, 2$ and the parameters β and μ specify the duration of the pulses β^{-1} and their spectral width $2\mu\beta$. Such pulses allow the efficient inversion of the ensemble of atoms with resonance frequencies in the spectral range $2\mu\beta$. To take into account the nonlinear transfer function of the acousto-optic modulator when forming these pulses, we fed a compensated-shape pulse to the input of the acousto-optic modulator in order to obtain
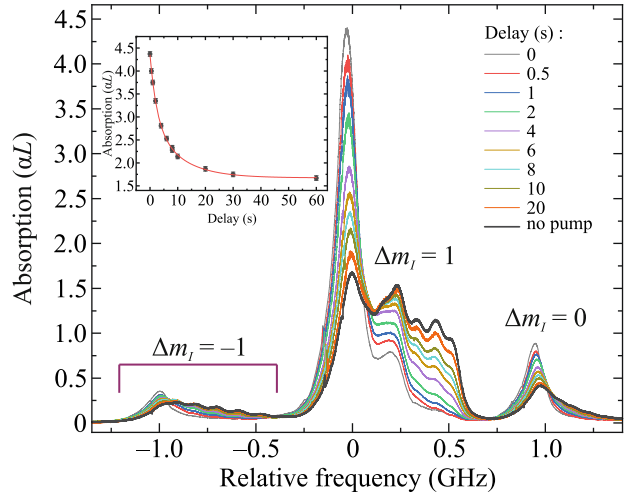
the output intensity $I_p(t) \sim \varepsilon_p^2(t) = \varepsilon_0^2 \text{sech}^2(\beta(t - t_p))$. The central frequencies of the burning pulses $\omega_{0,p}$ were specified to the left ($p = 1$) and to the right ($p = 2$) of the OQM working interval in the form

$$\omega_{(0,p)} = \omega_0 + 0.5\Delta(-1)^p, \tag{3}$$

where ω_0 is the central frequency of the signal pulse and $\Delta = 2$ MHz is the distance between the centers of the spectral dips, which exceeds the spectral width of the pulse ($\delta\omega = 2\mu\beta = 1$ MHz, $\beta = 2\pi \times 50$ kHz, and $\mu = 10$) corresponding to the width of the prepared spectral dips. The action of the sequence of two pulses took a time of 100 µs and was repeated 5000 times. Most of the Er ions immediately after the preparation of the absorption spectrum were in the optically excited state. The subsequent luminescence from this state resulted in the appearance of quantum noise with the simultaneous emission of the ROSE signal. To suppress the luminescence, we introduced an additional waiting time $\tau_w \approx 10 T_{1\,opt}$ (where $T_{1\,opt} \sim 10$ ms is the lifetime of the $^4I_{13/2}(0)$ excited state), during which the overwhelming number of ions transit from the excited to the ground states. In this case, the waiting time τ_w was 100 ms.
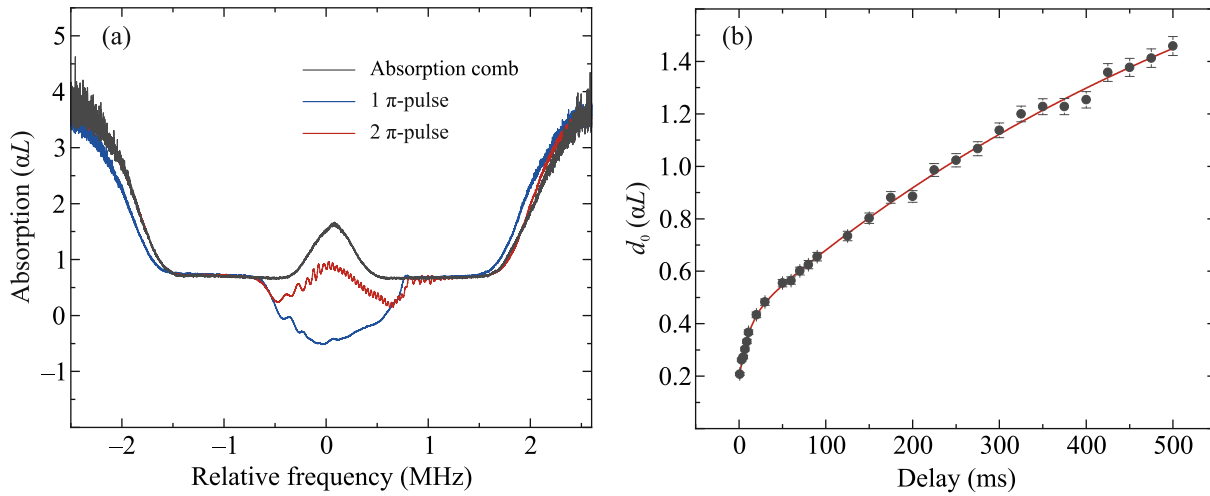
Fig. 4. (Color online) (a) Absorption line prepared with the sequences of laser pulses shown in Figs. 2a, 2b, and 2d (black line) without rephasing pulses and with (blue line) one and (red line) two rephasing pulses in the $^{167}Er^{3+}:Y_2SiO_5$ crystal ($c = 0.005\%$, $T = 1.3$ K). (b) Recovery of residual absorption in the frequency range of $1-2$ MHz from panel (a) versus the additional waiting time τ_w.

The spectrum of the resulting structure is shown by the black line in Fig. 4a. The observed absorption peak near the center of the line corresponds to the optical density $\alpha L_{peak} = 1.65$, and the FWHM of the absorption peak is 250 kHz, which coincides with the spectral width of the input signal pulse. The absorption intensity at the translucence on sides of the central absorption peak decreases to the residual level d_0 determining the optical density $\alpha_L = 0.65$, which noticeably depends on the additional waiting time τ_w. The dependence of residual absorption d_0 on the dependence of the additional waiting time τ_w is shown in Fig. 4b, where the red solid line is the approximation of the behavior of d_0 by the sum of two exponentials with the characteristic times $T_{1\,opt} = 10$ ms and $T_1 = 600$ ms. These times are in agreement with the relaxation times presented in [25] for the first impurity center in the $^{167}Er^{3+}:Y_2SiO_5$ crystal at a temperature of $T = 1.6$ K in the absence of the external magnetic field. The ratio of the absorption intensity at the central frequency of the signal pulse αL_{peak} to the residual absorption level d_0 at the edges of the peak $\alpha L_{peak}/d_0 = 2.5$, which allowed one to reduce quantum noise induced by the luminescence of ions with excited states that remain partially populated and optical transitions from which have frequencies beyond the spectral range of the signal pulse. At the same time, the reduction of the residual absorption level is an important problem, particularly, with a further increase in the efficiency of the input signal recovery when the OQM cell is placed in the optical cavity in the impedance-matching regime. To this end, the sequence of light pulses proposed in [24] can be used. Its experimental implementation is more difficult, but it ensures a quite low residual absorption

level of about $d_0 = 0.1$ without a decrease in the optical density in the center of the absorption line αL_{peak}.

According to the ROSE protocol, two rephasing pulses with the same carrier frequency coinciding with the central frequency of the optical transition ω_0 were fed to the crystal after the signal pulse. In our experiments, the parameters of rephasing pulses were specified in the same form (Eqs. (1) and (2)) with the parameters $\beta = 2\pi \times 50$ kHz and $\mu = 10$ so that the range of variation of the frequency of probe pulses covers the spectrum of the signal pulse (250 kHz). After the first rephasing pulse, a significant inversion of the populations of the levels involved in the optical transition in the ensemble of erbium ions in the frequency detuning range from -0.5 MHz to 0.5 MHz is observed (blue line in Fig. 4a). After the second rephasing pulse, absorption recovered to a level of $\alpha L \sim 1.0$ in the working spectral range of signal pulses (~ 250 kHz) (see the red line in Fig. 4a). This absorption level corresponded to the translucence of the optical transition at which the inversion of the atomic transition is absent. For this reason, the ROSE signal propagating in such a medium was not enhanced and, correspondingly, additional quantum noise generated by the echo signal enhancement does not appear.

It is also noteworthy that absorption in the spectral range of signal pulses is almost constant when controlled laser pulses with amplitude and frequency modulation are used, which ensures the conservation of the shape of the echo signal. The edges of the spectrum include residual translucence regions, which slightly affect the spectral dispersion but contribute to the optical quantum noise induced by the luminescence of ions in the same spectral range. At the same time, owing to the prepared structure of the absorp-
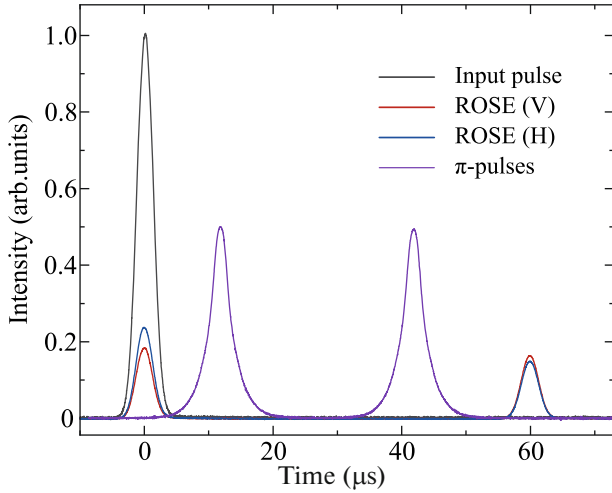
Fig. 5. (Color online) (Blue and red lines) ROSE signal in the $^{167}\text{Er}^{3+}$:Y_2SiO_5 crystal ($c = 0.005\%$, $\lambda \sim 1538.35$ nm, $H = 3.39$ T, $T = 1.3$ K) at $t = 60$ μs for the (blue line) horizontal ($\mathbf{E}_s \parallel D_1 \parallel \mathbf{H}$, $\mathbf{E}_s \parallel b$) and (red line) vertical ($\mathbf{E}_s \parallel D_1 \parallel \mathbf{H}$, $\mathbf{E}_s \parallel D_2$) polarization of signal radiation. The efficiency of echo revival is 15 and 17% in the case of horizontal and vertical polarization for a storage time of 60 μs, respectively. The black solid line at $t = 0$ is the input pulse and the blue and red solid lines are its part unabsorbed in the crystal in the case of horizontal and vertical polarization, respectively.

tion line, the ratio of integrated absorption in the residual translucence regions in the spectral range of the signal pulse [−0.25 MHz; 0.25 MHz] and in the spectral edges [−0.75 MHz; −0.25 MHz] and [0.25 MHz; 0.75 MHz] (see Fig. 4a) is a factor of 3 larger than a similar ratio in [20].

Figure 5 presents experimental data on the implementation of the ROSE protocol for the signal pulse that has the vertical ($\mathbf{E}_s \parallel D_2$) or horizontal ($\mathbf{E}_s \parallel b$) polarization and contains about 10^8 photons. The signal pulse had a Gaussian profile and a duration of 4 μs (black line at $t = 0$ in Fig. 5). The red and blue lines in Fig. 5 are the unabsorbed part of the signal pulse with the vertical ($\mathbf{E}_s \parallel D_2$) and horizontal ($\mathbf{E}_s \parallel b$) polarization at the input of the OQM cell, respectively. The rephasing pulses were applied at the times $t = 15$ and 45 μs (blue line in Fig. 5). The efficiency of signal recovery η is defined as the ratio of the energy of the echo signal to the energy of the input pulse. The recovery efficiency of the signal pulse with the vertical and horizontal polarization in our experiments at a storage time of 60 μs is 17 and 15% (see red and blue line in Fig. 5), respectively. The coherence time of the optical transition was $T_M = 123$ μs ($x = 1.35$), where T_M is the phase memory time determined within the Mims phase relaxation model [26]. The efficiency of signal recovery in the implemented ROSE protocol for the identical area θ_c of rephasing pulses can be estimated

using the equation for the pulse area of the ROSE signal [17]. The solution of this equation in the considered case of the orthogonal propagation of signal and rephasing pulses has the form

$$\eta(\alpha L, \theta_c) = e^{-2\left(\frac{2\tau}{T_M}\right)^x} \sin^8 \frac{\theta_c}{2} F(\alpha L, \theta_c)^2, \qquad (4)$$

where the function $F(\alpha L, \theta) = \alpha L \dfrac{\sinh\left\{\dfrac{\alpha L}{4}\sin^2\theta_c\right\}}{\left\{\dfrac{\alpha L}{4}\sin^2\theta_c\right\}} \times$

$e^{-\frac{(1+\cos^2\theta_c)\alpha L}{4}}$ characterizes the emission of the echo signal with the phased component of the resonance polarization whose maximum amplitude in the medium is proportional to $e^{-\left(\frac{2\tau}{T_M}\right)^x} \sin^4 \frac{\theta_c}{2}$. The solution given by Eq. (4) in the limit $\theta_c \to \pi$ (ideal rephasing pulses) describes the known case of the maximum possible efficiency of ROSE $\eta_{max}(\alpha L) = (\alpha L)^2 e^{-\alpha L} \times$ $e^{-2\left(\frac{2\tau}{T_M}\right)^x}$ [27], which does not exceed 25% at $\alpha L = 1.65$, $T_M = 123$ μs ($x = 1.35$), and $\tau = 30$ μs because of the reabsorption of the echo signal in the medium. The analysis of Eq. (4) shows that a small deviation of θ_c from π slightly affects the efficiency of the protocol. The efficiencies of ROSE obtained experimentally for two orthogonal polarizations of light pulses are $\eta(\alpha L, \theta_c) = 0.15$ and 0.17, which correspond to the area of control pulses $\theta_c \approx 0.7\pi$. To verify this value, we independently estimated the efficiency of rephasing pulses from the absorption measured with probe radiation (Fig. 4a), which was fed to the crystal after the first and second control pulses. The corresponding estimate is $\theta_c \approx 0.66\pi$, which indicates that the results obtained are reliable, the basis parameters of the ROSE protocol can be further improved, and its application for the efficient storage of polarization states of light is promising [28, 29].

Then, we implemented the ROSE protocol for OQM with the input signal pulse, which contained ~38 photons on average. Figure 6 presents histograms of counts of the single-photon detector averaged over a storage time of 17 min. The black line at $t = 0$ corresponds to the input signal pulse. After the application of two rephasing pulses at the times $t = 15$ and 45 μs, the ROSE signal was observed, which contained about 6 photons on average (see the red line at the time $t = 60$ μs). The efficiency of ROSE is 15%, which coincides with the efficiency of recovery of intense pulses (see Fig. 5). Quantum noise in the duration of the echo signal (4 μs) contained 4.5 photons on average. These experimental data show that appearing optical quantum noise is due only to the spontaneous
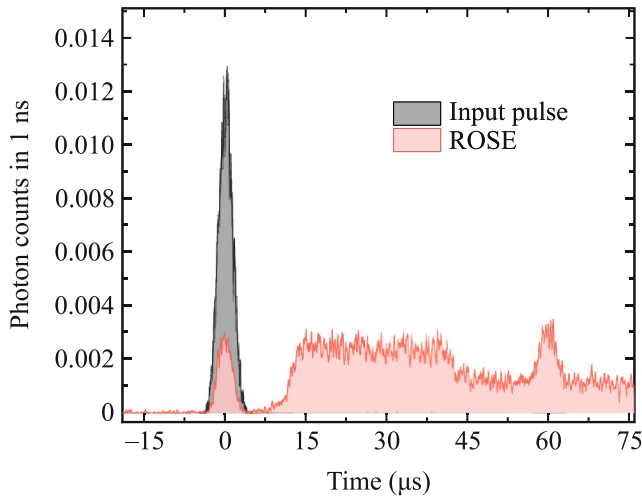
Fig. 6. (Color online) Histogram of counts of the single-photon detector. The gray histogram at $t = 0$ is the input pulse $\mathbf{E}_s \parallel D_1 \parallel \mathbf{H}$, $\mathbf{E}_s \parallel D_2$ (38 photons on average per 4 μs), the red histogram at $t = 0$ is the unabsorbed part of the input signal containing about 9 photons, and the red histogram at $t = 60$ μs is the ROSE signal containing 6 photons on average per 4 μs. The efficiency of echo revival is 15.9%. Spontaneous emission noise in an echo signal duration of 4 μs contained 4.5 photon on average. In the case of one rephasing pulse, noise consisted of about 9.3 photons per 4 μs.

emission from ions remaining in the excited state after the action of two imperfect rephasing pulses. The efficiency of input signal recovery in this work is smaller than that in [20] primarily because of a shorter coherence time of the optical transition and a smaller area of rephasing pulses. At the same time, the proposed preparation of the initial state of erbium ions allowed us to reduce quantum noise in the ROSE protocol by an order of magnitude, which open new possibilities of its further improvement.

To summarize, we have experimentally implemented optical quantum memory based on the modified revival of silenced echo (ROSE protocol). The initialization of the initial absorption line and the orthogonal geometry of the propagation of signal and rephasing pulses have reduced optical quantum noise induced by spontaneous emission from excited ions by almost an order of magnitude compared to the results obtained in [20] for the ROSE protocol. The implemented optical quantum memory scheme also allows the conservation of an arbitrary polarization of the signal pulse. Several methods can be proposed for the further improvement of the basis parameters in the conservation of the signal pulse, in particular, an increase in the signal-to-noise ratio. First, the coherence of the optical transition can be rephased on depleted levels involved in the optical transition using additional light pulses (e.g., at the transition between the $|-5/2\rangle_g$ and $|-5/2\rangle_e$ states). The authors of [30] showed that the rephasing of coherence on the transi-

tion adjacent to the signal one in the $Eu^{3+}:Y_2SiO_5$ crystal and the use of the selective filter in this crystal reduce quantum noise during the emission of the ROSE signal by a factor of more than 600; in this case, the coherence time between hyperfine states of erbium ions can reach several seconds [23]. Second, the application of a sequence of radio-frequency dynamic decoupling pulses on these transitions [31−33] will allow a significant increase in the storage time of optical quantum memory necessary for use in the quantum repeater. Third, the efficiency of initial signal recovery can be increased by using a higher quality $^{167}Er^{3+}:Y_2SiO_5$ crystal ensuring an increase in the coherence time of the optical transition. In particular, the authors of [23, 34] demonstrated that the coherence time of the optical transition under similar experimental conditions is $T_2 \sim 1$ ms. The efficiency can be further increased ($\eta > 64\%$) by placing the crystal in an optical cavity in the impedance-matching regime. We also note that integrated structures were formed in this crystal, in particular, a photonic crystal cavity [35, 36] and waveguide structures fabricated by femtosecond laser printing with both ends of the waveguide are directly connected with fiber arrays [37]. These waveguide structures can be considered as actual integrated optical quantum memory devices because transmission losses are less than 50%. These devices can be successfully integrated into the existing quantum communication channels.

FUNDING

CONFLICT OF INTEREST

The authors declare that they have no conflicts of interest.

OPEN ACCESS

REFERENCES

1. K. Heshami, D. G. England, P. C. Humphreys, P. J. Bustard, V. M. Acosta, J. Nunn, and B. J. Sussman, J. Mod. Opt. **63**, 2005 (2016).

2. N. Sangouard, C. Simon, H. de Riedmatten, and N. Gisin, Rev. Mod. Phys. **83**, 33 (2011).

3. F. Bussières, N. Sangouard, M. Afzelius, H. de Riedmatten, and W. Tittel, J. Mod. Opt. **60**, 1519 (2013).

4. T. Chanelière, G. Hétet, and N. Sangouard, Adv. At., Mol. Opt. Phys. **67**, 77 (2018).

5. A. I. Lvovsky, B. C. Sanders, and W. Tittel, Nat. Photon. **3**, 706 (2009).

6. S. A. Moiseev and S. Kroll, Phys. Rev. Lett. **87**, 173601 (2001).

7. W. Tittel, M. Afzelius, T. Chaneliére, R. L. Cone, S. Kröll, S. A. Moiseev, and M. Sellars, Laser Photon. Rev. **4**, 244 (2009).

8. V. Damon, M. Bonarota, A. Louchet-Chauvet, T. Chaneliére, and J.-L. le Gouët, New J. Phys. **13**, 093031 (2011).

9. J. Ruggiero, J.-L. le Gouët, C. Simon, and T. Chaneliére, Phys. Rev. A **79**, 053851 (2009).

10. H. Y. Carr and E. M. Purcell, Phys. Rev. **94**, 630 (1954).

11. M. Bonarota, J. Dajczgewand, A. Louchet-Chauvet, J.-L. le Gouët, and T. Chanelière, Laser Phys. **24**, 094003 (2014).

12. K. I. Gerasimov, M. M. Minnegaliev, S. A. Moiseev, R. V. Urmancheev, T. Chanelière, and A. Louchet-Chauvet, Opt. Spectrosc. **123**, 211 (2017).

13. X.-X. Li, P. Zhou, Y.-H. Chen, and X. Zhang, arXiv: 2203.03887v2 (2022).

14. V. Ranjan, Y. Wen, A. K. V. Keyser, S. E. Kubatkin, A. V. Danilov, T. Lindström, P. Bertet, and S. E. de Graaf, Phys. Rev. Lett. **129**, 180504 (2022).

15. A. Arcangeli, A. Ferrier, and P. Goldner, Phys. Rev. A **93**, 062303 (2016).

16. M. M. Minnegaliev, K. I. Gerasimov, R. V. Urmancheev, A. M. Zheltikov, and S. A. Moiseev, Phys. Rev. B **103**, 174110 (2021).

17. S. A. Moiseev, M. M. Minnegaliev, E. S. Moiseev, K. I. Gerasimov, A. V. Pavlov, T. A. Rupasov, N. N. Skryabin, A. A. Kalinkin, and S. P. Kulik, Phys. Rev. A **107**, 043708 (2023).

18. C. Liu, Z.-Q. Zhou, T. Zhu, L. Zheng, M. Jin, X. Liu, P.-Y. Li, J. Huang, Y. Ma, T. Tu, T.-S. Yang, C.-F. Li, and G. Guo, Optica **7**, 192 (2020).

19. J. Dajczgewand, J.-L. Le Gouët, A. Louchet-Chauvet, and T. Chanelière, Opt. Lett. **39**, 2711 (2014).

20. M. M. Minnegaliev, K. I. Gerasimov, T. N. Sabirov, R. V. Urmancheev, and S. A. Moiseev, JETP Lett. **115**, 720 (2022).

21. F. de Seze, F. Dahes, V. Crozatier, I. Lorgeré, F. Bretenaker, and J. L. le Gouët, Eur. Phys. J. D **33**, 343 (2005).

22. F. Könz, Y. Sun, W. Thiel, L. Cone, W. Equall, L. Hutcheson, and M. Macfarlane, Phys. Rev. B **68**, 1 (2003).

23. M. Rančić, M. P. Hedges, R. L. Ahlefeldt, and M. J. Sellars, Nat. Phys. **14**, 50 (2017).

24. J. S. Stuart, M. Hedges, R. Ahlefeldt, and M. Sellars, Phys. Rev. Res. **3**, L032054 (2021).

25. S. Yasui, M. Hiraishi, A. Ishizawa, H. Omi, T. Inaba, X. Xu, R. Kaji, S. Adachi, and T. Tawara, Opt. Contin. **1**, 1896 (2022).

26. W. B. Mims, Phys. Rev. **168**, 370 (1968).

27. N. Sangouard, C. Simon, M. Afzelius, and N. Gisin, Phys. Rev. A **75**, 032327 (2007).

28. T.-X. Zhu, C. Liu, M. Jin, M.-X. Su, Y.-P. Liu, W.-J. Li, Y. Ye, Z.-Q. Zhou, C.-F. Li, and G.-C. Guo, Phys. Rev. Lett. **128**, 180501 (2022).

29. B. I. Bantysh, K. G. Katamadze, Y. I. Bogdanov, and K. I. Gerasimov, JETP Lett. **116**, 29 (2022).

30. Y.-Z. Ma, M. Jin, D.-L. Chen, Z.-Q. Zhou, C.-F. Li, and G.-C. Guo, Nat. Commun. **12**, 4378 (2021).

31. G. Heinze, C. Hubrich, and T. Halfmann, Phys. Rev. Lett. **111**, 033601 (2013).

32. Y. Ma, Y.-Z. Ma, Z.-Q. Zhou, C.-F. Li, and G.-C. Guo, Nat. Commun. **12**, 2381 (2021).

33. S. A. Moiseev and V. A. Skrebnev, J. Phys. B: At. Mol. Opt. Phys. **48** (13) (2015).

34. M. Rančić, PhD Thesis (Australian Natl. Univ., Canberra, 2018).
https://doi.org/10.25911/5d67b2f1ee8f3

35. A. M. Dibos, M. Raha, C. M. Phenicie, and J. D. Thompson, Phys. Rev. Lett. **120**, 243601 (2018).

36. S. Chen, M. Raha, C. M. Phenicie, S. Ourari, and J. D. Thompson, Science (Washington, DC, U. S.) **370**, 592 (2020).

37. D. Liu, P.-Y. Li, T. Zhu, L. Zheng, J. Huang, Z.-Q. Zhou, C.-F. Li, and G.-C. Guo, Phys. Rev. Lett. **129**, 210501 (2022).

Translated by R. Tyapaev